Resonance Raman Spectroscopy of Uranocene: Observation of an Anomalously Polarized Electronic Band and Assignment of Energy Levels

R. F. Dallinger, P. Stein, and T. G. Spiro*

Contribution from the Department of Chemistry, Princeton University, Princeton, New Jersey 08540. *Received May 3, 1978*

Abstract: Raman spectra of uranocene obtained with tunable dye laser excitation, in the region of the visible charge transfer transitions, contain polarized bands at 211 and 754 cm^{-1}, assigned to ring-metal-stretching and ring-breathing modes, and an anomalously polarized band at 466 cm^{-1}, assigned to an electronic transition because of its lack of deuterium shift. Circular polarization measurements establish that $\Delta M_J = \pm 1$ for this transition. A reanalysis of the magnetic susceptibility data indicates that the uranocene ground state is the $M_J = \pm 4$ level of the $^3H_4$ manifold and that the first excited state is the 466-cm^{-1} level, with $M_J = \pm 3$. The polarizations of the charge transfer transitions are deduced from the Raman polarizations. The vibrational modes are resonant with the z-polarized but not the x,y-polarized transitions. For the highest energy charge transfer state, appreciable origin shifts are inferred from the 0-1 intensity of the ring-breathing mode and the overtone intensity of the metal-ring stretch. This state is split by 160 cm^{-1}, as determined by a quantitative fit of the 466 cm^{-1} mode intensity data. An excited state Jahn-Teller effect is suggested. A remarkable dispersion of the 466 cm^{-1} band depolarization ratio is shown to result from interference between scattering contributions from adjacent charge transfer states.

Uranocene, the bis(cyclooctatetraene) (COT) complex of uranium, has attracted much interest since its preparation and characterization by Streitwieser and Muller-Westerhoff.[1] It was the first extension of the π-sandwich compounds, exemplified by ferrocene, to the actinides, with their valence f orbitals. Streitwieser et al.[2] proposed a plausible bonding scheme involving overlap of the highest filled (e_{2u}) π orbitals of the COT^{2-} rings with the $l_z = \pm 2(f_{xyz}, f_{z(x^2-y^2)})$ uranium 5f orbitals. These overlaps are quite favorable, within the simple one-electron description, and they presumably account for the remarkable chemical and thermodynamic stability of uranocene.

A number of physical and spectroscopic studies provide some understanding of the role of the f electrons in ring-metal bonding and have been recently reviewed.[3] Several crystal field and molecular orbital calculations on uranocene[4-6] have been inconclusive in establishing its electronic structure, because of a lack of accurate crystal field parameters. The present study provides information relevant to establishing the nature of the low-lying f-orbital states as well as higher lying charge transfer states.

Uranocene is an attractive candidate for resonance Raman (RR) spectroscopy. It has well resolved and moderately intense visible absorption bands[2] which are attributable to charge transfer transitions from the COT^{2-} π orbitals to the uranium f orbitals. The molecular symmetry, D_{8h}, is very high, making polarization measurements especially useful. Despite the large number of atoms, there are only four totally symmetric vibrational modes: ring-metal stretching, ring breathing, and carbon-hydrogen stretching, and a perpendicular carbon-hydrogen bending. The first two are observed and readily identified in the RR spectra reported herein. In addition, we observe a third band, with anomalous polarization, which can be convincingly demonstrated to be an electronic Raman transition. Such transitions have normally been observed in solids at low temperatures,[7] but there have been two recent reports of electronic Raman bands in solution spectra.[8,9] These arise from transition metal ion d-d transitions and are quite broad. In contrast the uranocene electronic Raman band is narrow, consistent with its assignment to a transition between nonbonding 5f orbitals. Excitation profiles and polarizations of the three uranocene RR bands, together with a reanalysis of magnetic susceptibility data, provide a satisfying picture of several of the uranocene energy levels.

Experimental Section

Uranocene was a generous gift of Professor A. Streitwieser. It was dissolved in tetrahydrofuran (THF), which was distilled from sodium/benzophenone and then degassed by several freeze-pump-thaw cycles. Concentrations for the Raman experiments were $\sim 1 \times 10^{-3}$ M. Solutions were prepared in a Vacuum Atmospheres drybox and placed in a modified spinning cell equipped with a Teflon stopper immediately before the Raman experiments, even though the highly air-sensitive uranocene solution typically showed no decomposition in the spinning cell for several days.

Uranocene-d_{16} was prepared by the method of Streitwieser,[2] using cyclooctatetraene-d_8 from Merck & Co. as the starting material.

Laser excitation was obtained using a Coherent Radiation 490 dye laser pumped by a Spectra Physics 170 Argon laser. Rhodamine 6G, rhodamine B, and sodium fluorescein dyes were used. Raman spectra were taken with a Spex 1401 monochromator equipped with a cooled phototube and photon counting electronics.

Peak areas for excitation profiles were determined using a planimeter, with the 914 cm^{-1} THF solvent band used as a reference. The polaroid sheet analyzer used for the polarization measurements was checked using the 460 cm^{-1} ($\rho = 0$) and 314 cm^{-1} ($\rho = 0.75$) bands of CCl_4. Circular polarization measurements were obtained using a mica quarter-wave retardation plate and the optical arrangement described in ref 10.

For concentrated solutions, reabsorption effects on the relative intensities are large due to the sharpness of the absorption bands. The problem was minimized by lowering the concentration sufficiently such that the estimated corrections were <2.5% for $\lambda > 600$ nm and <10% for $\lambda < 600$ nm.

Results and Discussion

Vibrational Raman Bands. Laser excitation in the vicinity of the uranocene visible absorption bands produces a resonance Raman (RR) spectrum with three bands, at 211, 466, and 754 cm^{-1}. Figure 1 shows the spectrum obtained with 614.7-nm excitation. The 211- and 754-cm^{-1} bands are polarized, while the 466-cm^{-1} band is anomalously polarized ($\rho_l > 0.75$). The intensities vary rapidly with laser wavelength, and the excitation profile for the 466-cm^{-1} band is quite different from those of the 211- and 754-cm^{-1} bands (vide infra). This explains the fact that previous reports of uranocene Raman spectra appear to be contradictory. Karraker et al.[4] observed the 466-cm^{-1} band, using 632.8-nm excitation, while Hodgson et al.[11] observed the 211- and 754-cm^{-1} bands, with excitation that was presumably one of the Ar^+ lines in the blue or green region.

0002-7863/78/1500-7865$01.00/0

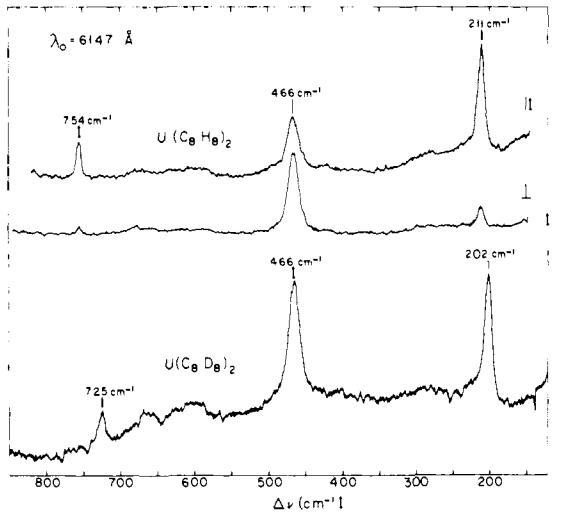

Figure 1. Resonance Raman spectra of uranocene ($U(C_8H_8)_2$, parallel and perpendicular components) and uranocene-d_{16} ($U(C_8D_8)_2$) in THF with 614.7-nm excitation. Conditions: spectral slit width = 6 cm^{-1}, time constant = 3 s, scan speed = 0.5 cm^{-1}/s, laser power ~175 mW, sensitivity ~1000 Hz, concentration ~1 mM.

Table I. Electronic Raman Tensor Patterns for Transitions within the $^3H_4$ Multiplet in a D_{8h} Crystal Field

$\begin{vmatrix} a & c & 0 \\ -c & a & 0 \\ 0 & 0 & b \end{vmatrix}$	$\begin{vmatrix} 0 & 0 & c \\ 0 & 0 & c \\ c' & c' & 0 \end{vmatrix}$	$\begin{vmatrix} a & c & 0 \\ c & -a & 0 \\ 0 & 0 & 0 \end{vmatrix}$
$\Delta M_J = 0$	$\Delta M_J = \pm 1$	$\Delta M_J = \pm 2$

Also shown in Figure 1 is the RR spectrum of uranocene-d_{16}. The 754- and 211-cm^{-1} bands shift down, by 29 and 9 cm^{-1}, respectively, on deuterium substitution, while the 466-cm^{-1} band is unshifted. The 754-cm^{-1} band is assigned to the ring-breathing mode, which is found at 737 cm^{-1} in cyclooctatetraene dianion.[12] Its deuterium shift is similar to those observed for the ring-breathing modes of ferrocene[13] and bis(benzenechromium).[14] The 211-cm^{-1} band is assigned to the symmetric metal-ring stretch, ν_{sym}. The asymmetric counterpart, ν_{asym}, is known from infrared data to be at 240 cm^{-1}.[15] For a linear triatomic model with point mass ligands (U = 238.03, C_8H_8 = 104.153) these frequencies are calculated[16] with a primary force constant k = 2.31 mdyn/Å, and a stretch-stretch interaction constant k' = 0.42 mdyn/Å. The predicted deuterium shift for ν_{sym} is 8 cm^{-1}, in excellent accord with the observed 9-cm^{-1} shift. The linear triatomic model has been used successfully for cyclopentadienyl sandwich complexes.[17] For ferrocene, values of k = 3.17 and k' = 0.54 mdyn/Å are obtained from ν_{sym} = 311 and ν_{asym} = 478 cm^{-1}. The smaller primary force constant of uranocene suggests a weaker metal-ring bond, consistent with the expected smaller overlap of f orbitals than d orbitals.

Electronic Assignment for the 466-cm^{-1} Band. The anomalous polarization observed for the 466-cm^{-1} band requires that its scattering tensor contain an antisymmetric contribution.[18,19] In the D_{8h} point group appropriate to uranocene[20] this is possible only for vibrations of a_{2g} and e_{1g} symmetry. Uranocene has one a_{2g} and five e_{1g} normal modes. The a_{2g} vibration involves in-plane C-H bending which should occur above 1000 cm^{-1}, and should shift markedly on deuterium substitution. The e_{1g} vibrations include three with substantial C-H bending character, a C-C stretch, and the symmetric ring-metal-ring tilt. All of them should be sensitive to deuterium substitution; the analogous modes in ferrocene[13] and bis(benzenechromium)[14] shift by at least 30 cm^{-1}.

The lack of deuterium shift renders any vibrational assignment of the 466-cm^{-1} band implausible. We assign it instead to an electronic transition. Electronic Raman bands are normally much broader than vibrational Raman bands[7] because of large vibronic contributions. As far as we are aware, this is the first observation of a narrow (~17 cm^{-1} bandwidth) electronic Raman band in solution. The assignment is reasonable for an "f-f" transition; such transitions, which are weakly coupled to molecular vibrations, are normally narrow.[21]

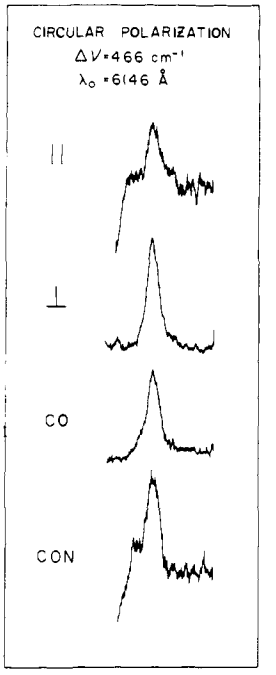

Figure 2. Circular polarization of the $\Delta\nu$ = 466 cm^{-1} mode of uranocene in THF with 614.6-nm excitation. Conditions: spectral slit width = 6 cm^{-1}, time constant = 3 s, scan speed = 0.5 cm^{-1}/s, laser power ~125 mW, sensitivity = 250 Hz, concentration ~1 mM. The features at the high-frequency (left) end of the || and CON components are due to glass scattering.

Uranocene contains U^{IV}, with a f^2 electronic configuration and a $^3H_4$ ground state.[3] This is split by the D_{8h} crystal field into five levels, with M_J = 0, ±1, ±2, ±3, and ±4. Electric polarizability selection rules allow Raman transitions for which ΔM_J = 0, ±1, or ±2 (i.e., ΔM_S = 0 and ΔM_L = 0, ±1, or ±2). The scattering tensors for these transitions are given in Table I. Antisymmetric contributions are possible only for ΔM_J = 0 or ±1.

Transitions with M_J = 0 have diagonal as well as antisymmetric off-diagonal scattering elements, while those with ΔM_J = ±1 have zero trace. These possibilities can be distinguished with the aid of circular as well as linear polarization measurements.[10,22] Figure 2 shows complete polarization measurements for the 466-cm^{-1} band, obtained in backscattering: parallel and perpendicular linear components ($I_\parallel$ and $I_\perp$) and co- and contrarotating circular components (I_{co} and I_{con}). The polarization components are related to the Raman tensor invariants as follows[18,19]

$$I_\parallel \doteq K(45\bar{\alpha}^2 + 4\gamma_s^2) \quad (1)$$

$$I_\perp = K(3\gamma_s^2 + 5\gamma_{as}^2) \quad (2)$$

$$I_{co} = K(6\gamma_s^2) \quad (3)$$

$$I_{con} = K(45\bar{\alpha}^2 + \gamma_s^2 + 5\gamma_{as}^2) \quad (4)$$

where K is an instrumental constant and the invariants are defined by:

$$\bar{\alpha}^2 = {}^1/_9(\sum\alpha^{\rho\rho})^2 \quad (5)$$

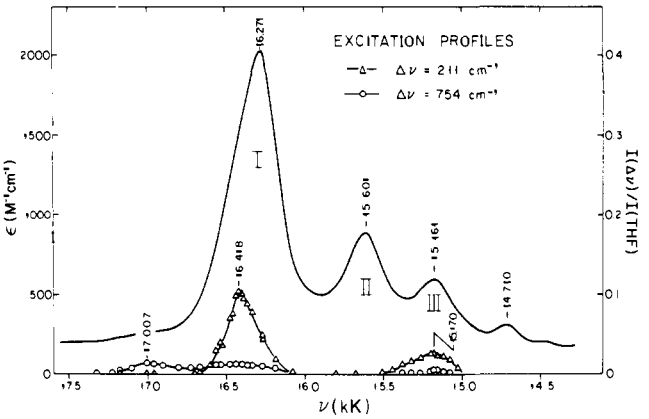

Figure 3. Absorption spectrum (solid line) of uranocene and excitation profiles for the 211-cm^{-1} (Δ) and 754-cm^{-1} (O) vibrational modes. The excitation profile is plotted as the ratio of the intensity of the uranocene Raman band to the intensity of the 914-cm^{-1} THF solvent band.

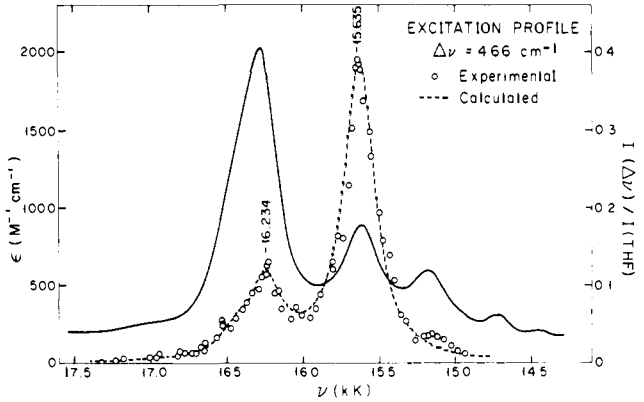

Figure 4. Excitation profile for the 466-cm^{-1} transition of uranocene. The solid line shows the absorption spectrum. The theoretical fit (dashed line) is calculated with eq 10 and parameters given in the text.

$$\gamma_s^2 = \tfrac{1}{2}\sum_{\rho\sigma}(\alpha^{\sigma\sigma} - \alpha^{\rho\rho})^2 + \tfrac{3}{4}\sum_{\rho\neq\sigma}^{\sigma\leq\rho}|\alpha^{\sigma\rho} + \alpha^{\rho\sigma}|^2 \quad (6)$$

$$\gamma_{as}^2 = \tfrac{3}{4}\sum_{\rho\sigma}^{\sigma\leq\rho}|\alpha^{\sigma\rho} - \alpha^{\rho\sigma}|^2 \quad (7)$$

where $\alpha^{\sigma\rho}$ is the $\sigma\rho$th component of the 3 × 3 scattering tensor.

Three polarization measurements are sufficient to determine the three tensor invariants, while the fourth measurement provides a check. The experimental intensities, $I_\parallel:I_\perp:I_{co}:I_{con}$ = 1.00:1.83:1.49:1.25, yield the following relative values of the invariants: $\gamma_s^2:\gamma_{as}^2:\bar{\alpha}^2$ = 1.00:0.88:0.0009. The propagation of an estimated 5% error in the intensity measurements yields a value for the trace of the tensor which is within experimental error of zero. This result identifies the 466-cm^{-1} band with a $\Delta M_J = \pm 1$ transition.

Excitation Profiles. The visible absorption spectrum of uranocene, shown in Figure 3, contains four well-resolved, fairly strong (ϵ = 300–2000 M^{-1} cm^{-1}) bands between 600 and 700 nm. Their separations are not the same, and do not correspond to vibrational frequencies. While f-f transitions are expected in this region of the spectrum they should be very much weaker. The most plausible assignment of the observed bands is to charge transfer transitions from filled π orbitals on the cyclooctatetraene rings to f orbitals on uranium. The weakly bonding character of the f orbitals could account for the relatively small (~250 cm^{-1}) bandwidths. (Ligand → metal charge transfer transitions terminating on d orbitals are usually quite broad.)

Also shown in Figures 3 and 4 are excitation profiles for the three Raman bands, obtained with tunable dye excitation. The available dyes (rhodamine 6G, sodium fluorescein, and rhodamine **B**) provided excellent coverage of the first three absorption bands, which we label I, II, and III in order of decreasing wavelength, but not the fourth. The experimental curves are striking. The two vibrational modes, 211 and 754 cm^{-1}, are in resonance with bands I and III, but show no enhancement under band II. In contrast, the 466 cm^{-1} electronic mode is maximally enhanced via band II, and to a lesser extent under band I, while band III gives no enhancement.

The 754-cm^{-1} profile shows an additional maximum about one vibrational quantum (~750 cm^{-1}) above the band I resonance, as expected for scattering from the 0-1 vibrational level of the excited state. The comparable 0-1 and 0-0 enhancements imply an appreciable origin shift of the excited state along the ring-breathing normal coordinate.[18] For the 211-cm^{-1} mode, the 0-0 and 0-1 separation is too small to be resolved in the excitation profile, but the intensity maximum is appreciably shifted (~150 cm^{-1}) from the band I maximum. This shift could be due to a substantial 0-1 intensity contribution. (The situation is further complicated by evidence, presented below, for a 120-cm^{-1} splitting of the electronic transition under band I.) For the 211-cm^{-1} mode, we were able to observe the first overtone, at 422 ± 3 cm^{-1}, as a shoulder on the 466-cm^{-1} band. Its intensity relative to the fundamental was found to be 0.12 ± 0.03. This leads to an estimate for the excited state ring-metal displacement, δ, of ~0.03 Å (about 1.5% of the ground state ring-metal distance, 1.92 Å)[23] using the relation[24] (appropriate for a linear triatomic molecule)

$$\delta = (\Delta/\pi)(Nh/cM_L\nu_{sym})^{1/2} \quad (8)$$

where N is Avogadro's number, h is Planck's constant, c is the velocity of light, M_L is the ligand mass (in amu), ν_{sym} is the vibrational frequency (in cm^{-1}), and Δ is the displacement parameter, which is here given approximately by $\Delta = (I_{overtone}/I_{fundamental})^{1/2}$.

Excited State Assignments. For the 211- and 754-cm^{-1} vibrational modes, the linear depolarization ratio is within experimental error of ⅓ and shows no dispersion with excitation wavelength. This is the value expected if only a single diagonal component of the scattering tensor has a nonnegligible value. For molecules such as uranocene with a threefold or higher rotation axis, z, symmetry requires that $\alpha^{xx} = \alpha^{yy}$ while α^{zz} is independent. The most reasonable way for the depolarization ratio to approach ⅓ in this situation is for α^{zz} to be the dominant tensor element. This requires bands I and III, with which the 211- and 754-cm^{-1} modes are resonant, to be z polarized. These excited states must have the same orbital angular momentum as the ground state, i.e., $\Delta M_J = 0$ (since $\Delta M_L = 0$ and $\Delta M_S = 0$). This inference is consistent with the MCD spectrum,[25] which shows only a weak inflection under band I.

The MCD spectrum shows a large inflection under band II,[25] implying a change in orbital angular momentum, and x,y polarization for the transition. The lack of resonance enhancement for vibrational modes implies little geometric distortion in this excited state. It is well coupled, however, to the 466-cm^{-1} electronic transition, for which ΔM_J is ±1. Band III disappears in low-temperature spectra[25] and is therefore a hot band.[26] Its separation from band II is 465 ± 15 cm^{-1}, the same energy as that of the electronic Raman transition.

These considerations are sufficient to establish the energy level scheme shown in Figure 5. The three electronic excited states, labeled f, e_{II}, and e_I at 466, 15 635, and 16 270 cm^{-1}, with $\Delta M_J = \pm 1$, ±1 and 0, respectively, account for the absorption bands I, II, and III, and for the electronic Raman band, resonant with bands I and II, but not band III. The two vibrational Raman bands are resonant with bands I and III.[26]

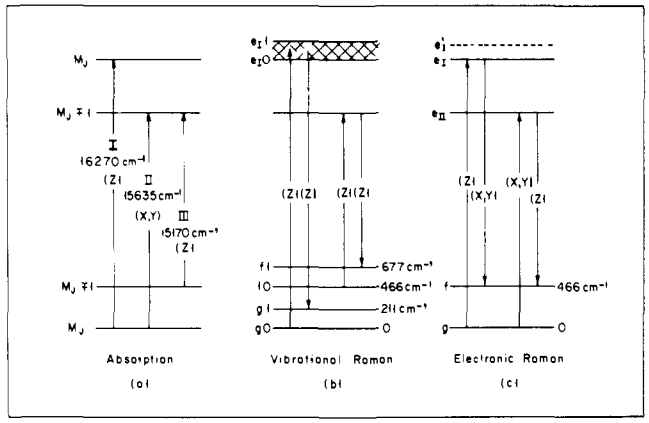

Figure 5. Energy level schemes for the optical and resonance Raman transitions of uranocene. g and f are two sublevels of the $^3H_4$ ground multiplet with M_J and $M_J \pm 1$, respectively. e_I (and e'_I) and e_{II} are components of the ligand–metal charge transfer state with M_J and $M_J \pm 1$. (a) Transitions associated with the absorption bands I, II, and III (see Figure 3), the polarizations being given in parentheses. (b) Raman transitions for the 211-cm^{-1} vibration, given by $g_0 \rightarrow g_1$ and $f_0 \rightarrow f_1$, where the latter arises due to thermal population of the f_0 level. (c) Raman pathways for the 466-cm^{-1} electronic Raman transition, which occur via the e_I (and e'_I) and e_{II} intermediate levels, the polarizations being given in parentheses.

Polarization Dispersion of the 466-cm^{-1} Mode. Although the 466-cm^{-1} mode is always anomalously polarized ($\rho_I > 3/4$), the values of the linear depolarization ratio vary markedly with excitation wavelength, as shown in Figure 6. At energies well above resonance, the values are very high, only the perpendicular component appearing with measurable intensity. As resonance is approached, ρ_I drops sharply, reaching a minimum value close to 3/4 between bands I and II, then rising steeply again. At resonance with either band I or band II, the value is close to two. This behavior is the inverse of that seen for porphyrin vibrational modes of mixed polarization in the region of Q-band resonance.[18,19,27,28,31] In that case, ρ_I reaches a maximum between the 0-0 and 0-1 vibronic levels, due to constructive interference between their antisymmetric scattering contributions and destructive interference between their symmetric contributions, and falls rapidly to zero outside the resonance region due to destructive interferences.

The present situation differs because the Raman transition involves two different electronic states. The resonant levels contribute asymmetric scattering terms which interfere destructively in the wavelength interval between them, and constructively elsewhere. This behavior can be understood with reference to the specific Raman pathways illustrated in Figure 5c. Scattering from excited state level e_I involves a z polarized incident photon and an x,y polarized scattered photon. The scattering tensor elements that are enhanced via band I are therefore α^{xz} and α^{yz}. For scattering from e_{II}, the polarization components are reversed, and α^{zy} and α^{zx} are enhanced. Either resonance in isolation would produce a depolarization ratio of 2.0 (via eq 1, 2, 6, and 7); this is close to the observed values at the centers of bands I and II.

The dispersion of the $\alpha^{\sigma\rho}$ element of the scattering tensor as given by second order perturbation theory is

$$\alpha_{fg}{}^{\sigma\rho} = \frac{1}{h}\sum_e \left[\frac{\langle f|\mu_\sigma|e\rangle\langle e|\mu_\rho|g\rangle}{\nu_{eg} - \nu_0 + i\Gamma e} + \frac{\langle f|\mu_\rho|e\rangle\langle e|\mu_\sigma|g\rangle}{\nu_{eg} + \nu_s + i\Gamma e}\right] \quad (9)$$

where μ_σ and μ_ρ are dipole moment operators with polarization directions σ and ρ, g and f are the initial and final states, e is an excited state of bandwidth Γ_e, ν_{eg} is the transition frequency, and ν_0 and ν_s are the frequencies of the incident and scattered photons. Near resonance the second term in eq 9 can be neglected. In the present case, we consider two nearby contributions in the summation, e_I and e_{II}.

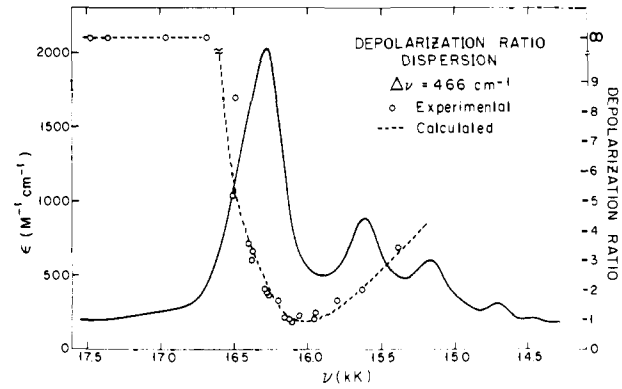

Figure 6. Dispersion of the linear depolarization ratio for the 466-cm^{-1} transition of uranocene. The solid line shows the absorption spectrum. The theoretical fit (dashed line) is calculated with eq 11 and parameters given in the text.

The intensity and depolarization ratios become

$$I = (3/2)K[7|\alpha^{xz} + \alpha^{zx}|^2 + 5|\alpha^{xz} - \alpha^{zx}|^2] \quad (10)$$

and

$$\rho_I = 3/4 + 5/4\left[\frac{|\alpha^{xz} - \alpha^{zx}|^2}{|\alpha^{xz} + \alpha^{zx}|^2}\right] \quad (11)$$

where

$$\alpha^{xz} = 1/h\left[\frac{N_I}{(\nu_{e_Ig} - \nu_0 + i\Gamma_{e_I})}\right]$$

$$\alpha^{zx} = 1/h\left[\frac{N_{II}}{(\nu_{e_{II}g} - \nu_0 + i\Gamma_{e_{II}})}\right]$$

The numerators N_I and N_{II} (where $N_I = \langle f|\mu_{x,y}|e_I\rangle\langle e_I|\mu_z|g\rangle$ and $N_{II} = \langle f|\mu_z|e_{II}\rangle\langle e_{II}|\mu_{x,y}|g\rangle$) are different. The larger enhancement observed from band II implies that $|N_I/N_{II}| < 1$.

The denominators change signs at resonance. At wavelengths between the e_I and e_{II} resonances, the two terms will have opposite signs if the signs of N_I and N_{II} are the same; they will have the same signs if the signs of N_I and N_{II} are opposite. The latter situation must apply, since the depolarization ratio approaches 3/4 (symmetric anisotropic scattering) between e_I and e_{II}; at this point $\alpha^{xz(yz)}$ and $\alpha^{zx(zy)}$, having reached the same magnitude, must also have the same sign. At energies higher than e_I or lower than e_{II} the resonance denominators have the same sign, and the opposite signs of N_I and N_{II} produce the antisymmetric combination of the scattering tensor elements. Consequently, ρ_I rises above two. Since $|N_I/N_{II}| < 1$, there will be some point on the high-energy side where $\alpha^{zx(zy)}$ approaches $-\alpha^{xz(yz)}$ and ρ_I approaches infinity. At still higher energies $\alpha^{zx(zy)} > -\alpha^{xz(yz)}$, as the importance of the resonance denominators diminish, and ρ_I is predicted to fall again (although the intensity may be too low to allow the prediction to be checked). On the low-energy side $\alpha^{zx(zy)} > -\alpha^{xz(yz)}$ for all energies; ρ_I is predicted to reach a finite maximum and then decrease again.

Splitting of e_I. The dashed lines of Figures 4 and 6 are the 466-cm^{-1} excitation profile and depolarization dispersion calculated with eq 10 and 11. An accurate fit to the data required the assumption of a 160-cm^{-1} splitting of the e_I level into two unequal components, e_I and e_I'. The curves shown were calculated with the following parameters: $\nu_{e_{II}g} = 15\,630$ cm^{-1}, $\nu_{e_Ig} = 16\,260$ cm^{-1}, $\nu_{e_I'g} = 16\,420$ cm^{-1}, $\Gamma_{e_{II}} = \Gamma_{e_I} = \Gamma_{e_I'} = 120$ cm^{-1}, $N_I/N_{II} = -0.45$, and $N_I'/N_{II} = -0.18$.

The splitting of the e_I level is plausibly due to an excited state Jahn-Teller distortion. The charge transfer process proposed for this transition would place an electron in a degenerate pair of weakly antibonding 5f orbitals. The degeneracy would be

broken by a molecular distortion that destroyed the axial symmetry, e.g., a tilt or a slip of the cyclooctatetraene rings. The vibrational mode leading to this distortion would be subject to resonance enhancement, but the frequency might be too low to permit its detection.

Magnetic Susceptibility and the Ground State. The Raman data do not identify the ground state of uranocene, but they do restrict the possibilities for interpretation of the magnetic moment whose variation from $\mu_{eff} = 2.4\ \mu_B$ at ~10 K to $2.6\ \mu_B$ at room temperature[6] reflects contributions from low-lying excited states. Amberger et al.,[6] fitted their magnetic susceptibility data to a model with an $M_J = 0$ ground state and $M_J = \pm1, \pm2$ excited states at 17 and 200 cm^{-1}, respectively. This interpretation is inconsistent with the present finding of a $\Delta M_J = \pm1$ transition at 466 cm^{-1}, and also with magnetic data on substituted uranocenes.

The magnetic moment can be calculated for each of the M_J levels using the $\langle M_J|\kappa L_Z + 2S_Z|M_J\rangle = (^2/_5)M_J(3\kappa - 1)$ relation,[3] the matrix elements of the Zeeman operator where κ is the covalency reduction factor. The low-temperature value, $\mu_{eff} = 2.4\ \mu_B$, is obtainable for either $M_J = \pm4$ or ±3 with reasonable reduction factors, $\kappa = 0.84$ and 1.00, respectively. With $M_J = \pm2$ or ±1 unrealistic values of κ, substantially greater than unity, are required to obtain $\mu_{eff} = 2.4\ \mu_B$. The temperature variation of the magnetic susceptibility can be calculated with Van Vleck's formula[29] which includes the first and second Zeeman terms. For a two-level system the expression is

$$\chi = \frac{N\beta^2[\mu_I^2/kT + (\mu_{II}^2/kT)e^{-\omega/kT} + (4\mu_{I,II}^2/\omega)(1 - e^{-\omega/kT})]}{3(1 + e^{-\omega/kT})} \quad (12)$$

where μ_I and μ_{II} are the magnetic moment matrix elements from the ground and excited levels, $\mu_{I,II}$ is the off-diagonal matrix element (i.e., $\langle\pm4|\kappa L_x + 2S_x|\pm3\rangle = [2(2^{1/2})/5](3\kappa - 1)$ or $\langle\pm3|\kappa L_x + 2S_x|\pm2\rangle = [14^{1/2}/5](3\kappa - 1)$), N is Avogadro's number, β is the bohr magneton, and ω is the excited state energy, 466 cm^{-1} above the ground level. Since $\Delta M_J = \pm1$, this state is $M_J = \pm3$ if the ground state is $M_J = \pm4$. If the ground state is $M_J = \pm3$, then the excited state may be either $M_J = \pm4$ or ±2. Theoretical curves for these three possibilities are compared in Figure 7 with the susceptibility data of Amberger et al.[6] The fit for an $M_J = \pm4$ ground state is clearly superior to the other two possibilities. It would be improved even more with inclusion of a small contribution from a higher lying $M_J = \pm2$ level, which would lower $1/\chi$ slightly at higher temperatures. This conclusion is consistent with the interpretation of the NMR study of Edelstein et al.[30]

Some time ago, Karraker et al.[4] noted that the $M_J = \pm4$ level would lie lowest if the crystal field parameter B_0^2 is much larger than B_0^4 and B_0^6, as expected for a simple axial field. If this is the case, then the location of $M_J = \pm3$ at 466 cm^{-1} permits an estimate of $B_0^2 = 2112$ cm^{-1} and a prediction of the remaining levels at 799, 999, and 1065 cm^{-1} for $M_J = \pm2$, ±1, and 0, respectively, from the $(B_0^2/2)\langle M_J|(3\cos^2\theta - 1)|M_J\rangle$ matrix elements. The transition to $M_J = \pm2$ is Raman allowed and might be expected to be resonant with the e_{II} state, which would provide an intermediate level with $\Delta M_J = \pm1$ relative to both initial and final states. We searched the Raman spectra carefully in the region of 799 cm^{-1} but could find no evidence for another band. Perhaps the transition moment between the $M_J = \pm2$ level and e_{II} is too small to provide appreciable Raman intensity.

Conclusions

The following inferences about uranocene emerge from the resonance Raman data and the reanalysis of the magnetic susceptibility:

1. The ground state is the $M_J = \pm4$ level of the $^3H_4$ manifold.

2. The first electronic excited state is the $M_J = \pm3$ level, 466 cm^{-1} above the ground state. It gives rise to a sharp Raman band, which exhibits resonance enhancement and depolarization dispersion in the vicinity of the visible charge transfer bands.

3. The polarizations of three of the charge transfer bands, one of them a hot band with the 466-cm^{-1} level as its initial state, are deduced from the Raman polarizations. The symmetric metal-ring stretching and ring-breathing vibrations are enhanced via the z-polarized transitions. For the highest energy charge transfer state appreciable origin shifts are inferred from the 0-1 intensity of the ring-breathing mode and the overtone intensity of the metal-ring stretching mode.

4. The highest energy charge transfer state is split by 120 cm^{-1}, as determined from a quantitative fit of the 466-cm^{-1} mode excitation profile and depolarization dispersion. An excited state Jahn-Teller effect is suggested.

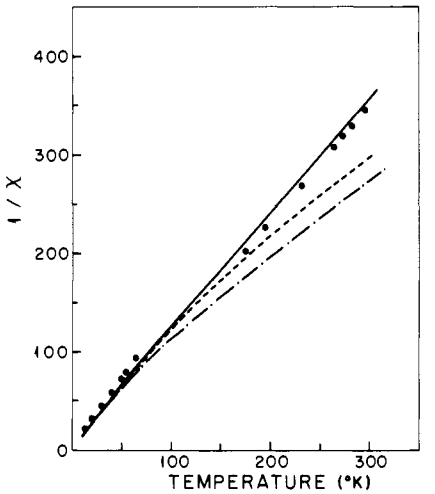

Figure 7. Temperature dependence of the reciprocal of the magnetic susceptibility for uranocene with the calculated fits assuming the following M_J values for the ground level and the 466-cm^{-1} excited level: (—) $M_J = \pm4$ ground level, $M_J = \pm3$ excited level, $\mu_{I,I} = 2.4$, $\mu_{II,II} = 1.83$, and $\mu_{I,II} = 0.86$; (- - -) $M_J = \pm3$ ground level, $M_J = \pm4$ excited level, $\mu_{I,I} = 2.4$, $\mu_{II,II} = 3.2$, and $\mu_{I,II} = 1.132$; (- · -) $M_J = \pm3$ ground level, $M_J = \pm2$ excited level, $\mu_{I,I} = 2.4$, $\mu_{II,II} = 1.6$, and $\mu_{I,II} = 1.5$; (· · ·) experimental data from the fit in ref 6 with Curie-Weiss relation $\chi = C/(T + \theta)$, using $C = 0.725$ and $\theta = 2.9$ below 100 K and $C = 0.85$ and $\theta = -3.0$ above 200 K.

Acknowledgment. We thank Professor A. Streitwieser for the sample of uranocene, Dr. J. Hare for helpful discussions, and Professor P. Schatz and Dr. R. Mowrey for communicating their MCD results to us. This work was supported by National Science Foundation Grant CHE 74-00055.

References and Notes

(1) A. Streitwieser and U. Muller-Westerhoff, *J. Am. Chem. Soc.*, **90**, 7364 (1968).
(2) A. Streitwieser, U. Muller-Westerhoff, G. Sonnichsen, F. Mares, D. G. Morrell, K. O. Hodgson, and C. A. Harmon, *J. Am. Chem. Soc.*, **95**, 8644 (1973).
(3) K. Warren, "Structure and Bonding", Vol. 33, Springer-Verlag, New York, N.Y., 1977, pp 97-138.
(4) D. G. Karraker, J. A. Stone, E. R. Jones, and N. Edelstein, *J. Am. Chem. Soc.*, **92**, 4841 (1970).
(5) R. G. Hayes and N. Edelstein, *J. Am. Chem. Soc.*, **94**, 8688 (1972).
(6) H. D. Amberger, R. D. Fischer, and B. Kanellakopulos, *Theor. Chim. Acta*, **37**, 105 (1975).
(7) J. A. Koningstein, *Mol. Spectrosc.*, **4**, 196 (1976).
(8) Y. Funato, T. Kamisuki, K. Ikeda, and S. Maeda, *J. Raman Spectrosc.*, **4**, 415 (1976).
(9) R. J. H. Clark and P. C. Turtle, *Chem. Phys. Lett.*, **51**, 265 (1977).
(10) M. Pezolet, L. A. Nafie, and W. Peticolas, *J. Raman Spectrosc.*, **1**, 455 (1973).
(11) K. O. Hodgson, F. Mares, D. F. Starks, and A. Streitwieser, *J. Am. Chem.*

Soc., 95, 8650 (1973).
(12) R. Dallinger, unpublished result.
(13) E. R. Lippincott and R. D. Nelson, *Spectrochim. Acta*, **10**, 307 (1958).
(14) S. J. Cyvin, J. Brunvoll, and L. Schafer, *J. Chem. Phys.*, **54**, 1517 (1971).
(15) L. Hocks, J. Goffart, G. Duyckaerts and P. Teyssie, *Spectrochim. Acta, Part A*, **30**, 907 (1974).
(16) G. Herzberg, "Infrared and Raman Spectra", Van Nostrand, New York, N.Y. 1945, p 154.
(17) D. M. Duggan and D. N. Hendrickson, *Inorg. Chem.*, **14**, 955 (1975).
(18) T. G. Spiro and P. Stein, *Annu. Rev. Phys. Chem.*, **28**, 501 (1977).
(19) T. G. Spiro and P. Stein, *Indian J. Pure Appl. Phys.*, **16**, 213 (1978).
(20) The analysis is unaffected if the point group is D_{8d} (staggered rings) rather than D_{8h} (eclipsed rings).
(21) C. K. Jorgensen, "Absorption Spectra and Chemical Bonding in Complexes", Pergamon Press, New York, N.Y., 1962, pp 173–178.
(22) J. R. Nestor and T. G. Spiro, *J. Raman Spectrosc.*, 1, 539 (1973).
(23) A. Avdeef, K. N. Raymond, K. O. Hodgson, and Z. Zalkin, *Inorg. Chem.*, 11, 1083 (1972).
(24) F. Inagaki, M. Tasumi, and T. Miyazawa, *J. Mol. Spectrosc.*, **50**, 286 (1974).
(25) R. L. Mowery, Ph.D. Thesis, University of Virginia, 1976.
(26) In principle, the vibrational energies for the excited state at 466 cm^{-1} are not the same as those of the ground state, so that a frequency shift might be expected for the vibrational modes resonant under band III. The excited state must have essentially the same bonding as the ground state, however, as evidenced by the narrowness of the 466-cm^{-1} mode, and vibrational shifts are expected to be negligible.
(27) O. S. Mortensen, *Chem. Phys. Lett.*, **30**, 406 (1975).
(28) S. Sunder, R. Mendelsohn, and H. J. Bernstein, *J. Chem. Phys.*, **63**, 573 (1975).
(29) J. H. Van Vleck, "The Theory of Electric and Magnetic Susceptibilities", Oxford University Press, New York, N.Y., 1948.
(30) N. Edelstein, G. N. Lamar, F. Mares, and A. Streitwieser, Jr., *Chem. Phys. Lett.*, **8**, 399 (1971).
(31) J. Friedman and R. M. Hochstrasser, *Chem. Phys. Lett.*, **32**, 414 (1975).

Chemically Modified Electrodes. 13. Monolayer/Multilayer Coverage, Decay Kinetics, and Solvent and Interaction Effects for Ferrocenes Covalently Linked to Platinum Electrodes

Jerome R. Lenhard and Royce W. Murray*

Contribution from the Kenan Laboratories of Chemistry, University of North Carolina, Chapel Hill, North Carolina 27514. *Received June 23, 1978*

Abstract: Surface synthesis, electrochemical properties, and second-order ferricinium decay kinetics are described for a series of ferrocene carboxylic acids immobilized on PtO surfaces using alkylaminesilane chemistry. For immobilized ferrocenylphenylacetamide, surface activity nonideality parameters are smaller and ferricinium stability is enhanced for immobilized multilayers as compared to monolayers.

The reactions which an electrode-immobilized molecular charge-transfer state can undergo during repetitive cycling between different oxidation states are pertinent to any eventual electrocatalytic utility. Appreciation of the various chemical stabilizing and destabilizing factors in the surface molecular structures is presently fragmentary. Efforts[1-6] have been both limited and hampered by modest chemical lifetimes of available surface structures plus poor definition (signal/background) of electrochemical electron-transfer responses. This paper describes the synthesis and properties of a series of ferrocenecarboxylic acids demonstrably covalently linked to electrogenerated Pt|PtO surfaces using the alkylaminesilane 3-(2-aminoethylamino)propyltrimethoxysilane (*en*-silane) and carbodiimide-assisted amidization (reaction 1). Ferrocenylphenylacetic acid, I, immobilized in this manner, exhibits remarkable chemical and electrochemical stability and well-defined cyclic voltammetric response. We present here quantitative information on decay kinetics of redox molecules immobilized on electrodes. The decay, interestingly, is second order in ferricinium. We also describe an analysis of interactions based on solvent and surface activity effects. We have prepared both monolayer and multilayer coverages of I on electrodes and report the first comparison of electrochemistry, chemical stability, and surface activity of a covalently linked molecule at monolayer and multilayer coverage.

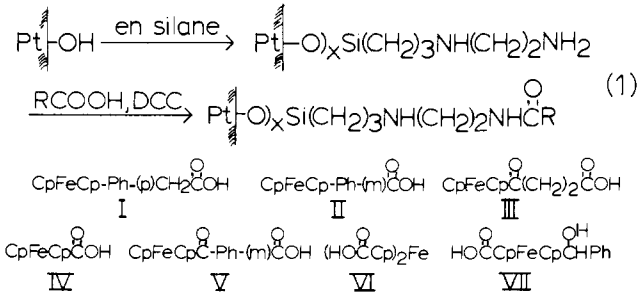

Experimental Section

Chemicals. 3-(2-Aminoethylamino)propyltrimethoxysilane (*en*-silane, PCR) was distilled when received and routinely redistilled thereafter. Acetonitrile (Spectrograde, MCB) was dried over molecular sieves and benzene over sodium. Dicyclohexylcarbodiimide (DCC, Aldrich) was used as received. Tetraethylammonium perchlorate (Eastman, recrystallized three times from water) was supporting electrolyte throughout.

All ferrocene compounds were courtesy of Professor W. F. Little (UNC, Chapel Hill) except IV and VI (Aldrich) and 1,1′-bis(trimethylsilyl)ferricinium tetrafluoroborate (from Professor M. Wrighton, MIT).

Apparatus. Current-potential waves were observed by cyclic voltammetry using electrochemical equipment and cells of conventional design. Potentials are referenced to a NaCl saturated calomel electrode (SSCE). Fast sweep data were obtained with a PARC Model 173 potentiostat and *iR* compensation. Pt disk electrodes (area 0.102 to 0.153 cm^2) were silver soldered to brass rods; some for interchangeable use in electron spectroscopy and electrochemical experiments were fitted with Teflon shrouds. X-ray (Mg anode) photoelectron spectra (XPES) were obtained with a DuPont 650B electron spectrometer,[7] data acquisition and manipulation on which were facilitated by a microprocessor system.[8] Intensities are expressed as integrated peak areas.

Procedure. Mirror polished (1 micron diamond paste) Pt disk electrodes are cleaned by 5-min anodization in 1 M H_2SO_4 (+1.9 V

0002-7863/78/1500-7870$01.00/0